Angle-dependent analysis and modeling of absorption and structural colors in feathers

Jiří Filip[1,*], Frank J. Maile[2] and Radomír Vávra[1]

[1]The Czech Academy of Sciences, Institute of Information Theory and Automation, Prague, Czech Republic
[2]Schlenk Metallic Pigments GmbH, Roth-Barnsdorf, Germany

Abstract

Bird feathers represent one of the most challenging examples of material appearance, driven by a combination of structural properties at different scales. At the microscopic scale, feather appearance is dictated by the anisotropic behavior of directional feather parts. At the nanoscale, some species exhibit structural color due to light diffraction on structures comparable in size to the wavelength of light. In this paper, we capture feathers from four different species, analyze various aspects of their appearance, and suggest its efficient modeling approach.

Keywords

Feather, Appearance, Structural color, BTF, BRDF, angle dependency

1. Introduction

The specific appearance of feathers allows for the introduction of glossy, metallic, or iridescent effects [1], which are related to specific pigments or structures within the feather parts. A typical feather consists of a central shaft (rachis), with serial paired branches (barbs) forming a flattened, usually curved surface called the vane (see Fig. 1). The barbs possess further branches called barbules. The barbules of adjacent barbs are attached to one another by hooks, stiffening the vane. In many birds, some or all of the feathers lack barbules or hooks, resulting in plumage with a loose, hairlike appearance [2].

Feather parts are made from keratin, and color effects in feathers arise from *absorption colors* produced by carotenoid, melanin, and porphyrin pigments, or from *structural colors*. Structural colors can lead to iridescent effects, such as those seen in hummingbirds, or to blue colors specifically observed in the serially paired branches called barbs. This is due to a unique porous structure with dimensions smaller than the wavelength of light.

Feathers are known for their intricate angle-dependent appearance, as demonstrated in Fig. 2. Although the composition of feathers and their relationship with color appearance have been deeply studied in recent years, the angle-dependent interaction of complex feather structures with lighting or observation from varying directions, and its simulation for appearance characterization and visualization purposes, remains an open research task.

CVCS2024: the 12th Colour and Visual Computing Symposium, September 5–6, 2024, Gjøvik, Norway
*Corresponding author.
filipj@utia.cas.cz (J. Filip)
https://staff.utia.cas.cz/filip (J. Filip)

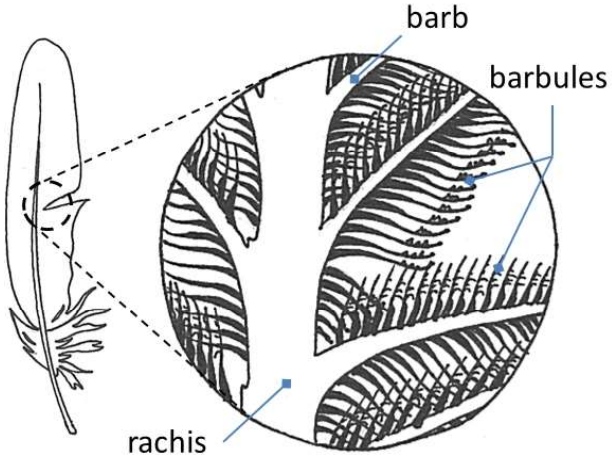

Figure 1: A scheme of typical feather structure.

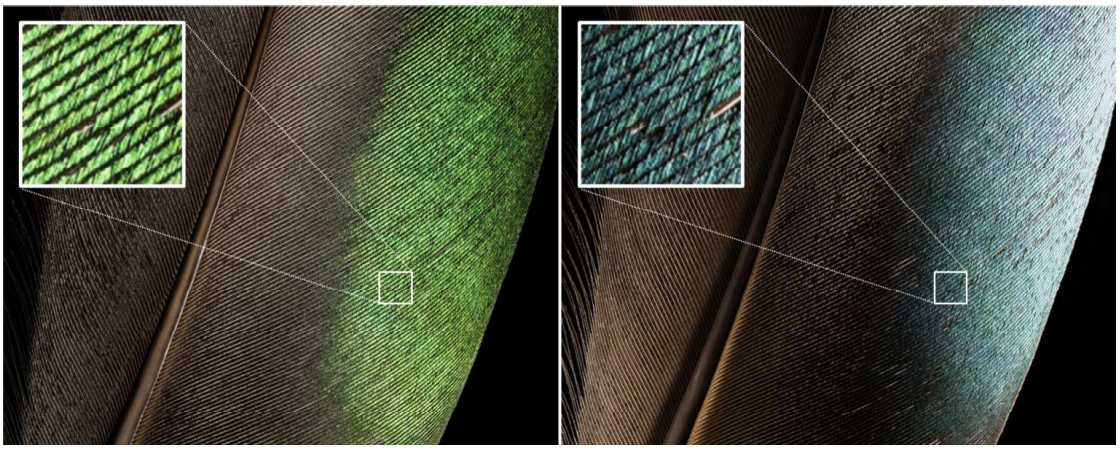

Figure 2: Pictures depicting the angle-dependent appearance of feather (maned or Australian wood duck, chenonetta jubata) by courtesy of Heidi & Hans-Jürgen Koch [3]).

In this paper, we examine the intricate details, including blue structural coloration, in bird feathers. We performed an angle-dependent analysis of feathers of four avian species. The main contributions of this work are the characterization of the angle-dependent appearance of feathers, specifically:

- Capturing high-resolution angle-dependent photographs of four feather samples.
- Explaining the details of the angular behavior including structural colors and their relationship to local aspects of the feather texture.
- Proposing a novel analytical reflectance model of major features of the feather textureless appearance.

2. Related Work

The principles of color in feathers were discussed as early as Newton [4], who suggested that peacock feathers "appear of several colors in several positions of the Eye" and that their color "arises from the thinness of the transparent parts of the Feathers." The physical principle of structural colors in feathers was first explained by Bancroft [5].

More recently, general principles of angle-dependent optical effects deriving from sub-micron structures of films and pigments were surveyed Pfaff and Reynders [6]. Srinivasarao [7] provides a comprehensive survey of nano-optics related color principles in the biological world, including beetles, butterflies, birds, and moths. Gruson et al. [8] suggested a straightforward method to characterize the angle-dependent effects of structural colors using spectrometry with an optimized set of geometries and five parameters: hue, angle dependence of hue, maximum brightness, tilting, and angle dependence of brightness. Maia et al. [9] have shown that feather gloss depends on the shape and structure of the keratin cortex of the barbules, and that glossy feathers are morphologically intermediate between matte black and iridescent feathers. Saranathan et al. [10] used synchrotron small-angle X-ray scattering and optical spectrophotometry to characterize the nanostructure and optical function of 297 distinctly colored feathers from 230 species, confirming the presence of a predominant, isotropic length scale of variation in refractive index that produces strong reinforcement of a narrow band of scattered wavelengths. Parnell et al. [11] studied Eurasian Jay feathers and explained the reasons for periodic variations in the reflected color of a single barb, ranging from white through light blue, dark blue, and black. Imafuku [12] characterized the angle-dependent behavior of butterfly wings. Structural colors have been thoroughly studied, and there are even attempts to mimic their appearance in practical industrial applications [13]. Magkiriadou et al. [14] introduced angle-independent structural colors by packing core-shell colloidal particles consisting of high-refractive-index cores and soft, transparent shells.

While the majority of the studies focused on the spectral behavior of feather parts under fixed viewing and illumination condition, we focus on the detailed characterization and modelling of feather appearance as a function of illumination and viewing angle.

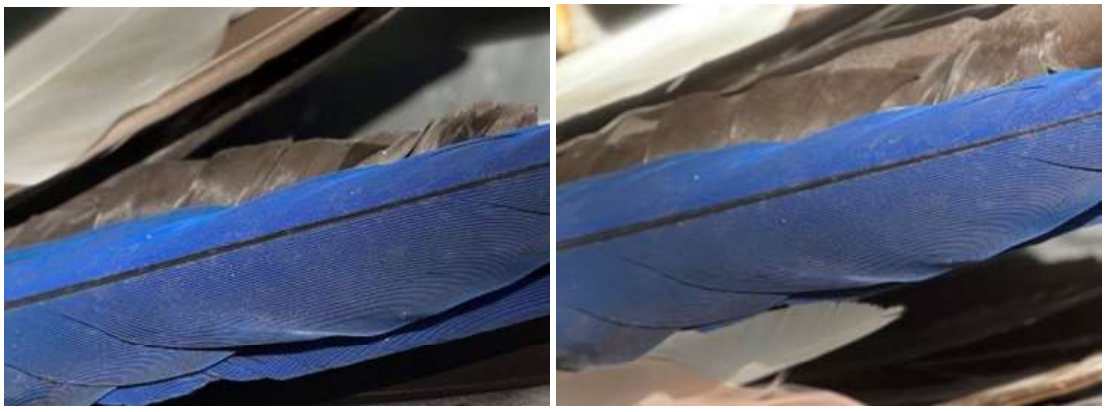

Figure 3: An example of angle-dependent effect of a macaw parrot feather.

3. Feather samples

We selected feathers from four distinct bird species covering different types of color formation principles (structural, absorption, and a combination) and an achromatic one. Therefore, our sample set contains *macaw parrot* (parrot), *Cochin cock* (rooster), *greater flamingo* (flamingo), and *white stork* (stork), as shown in the first row of Fig. 4.

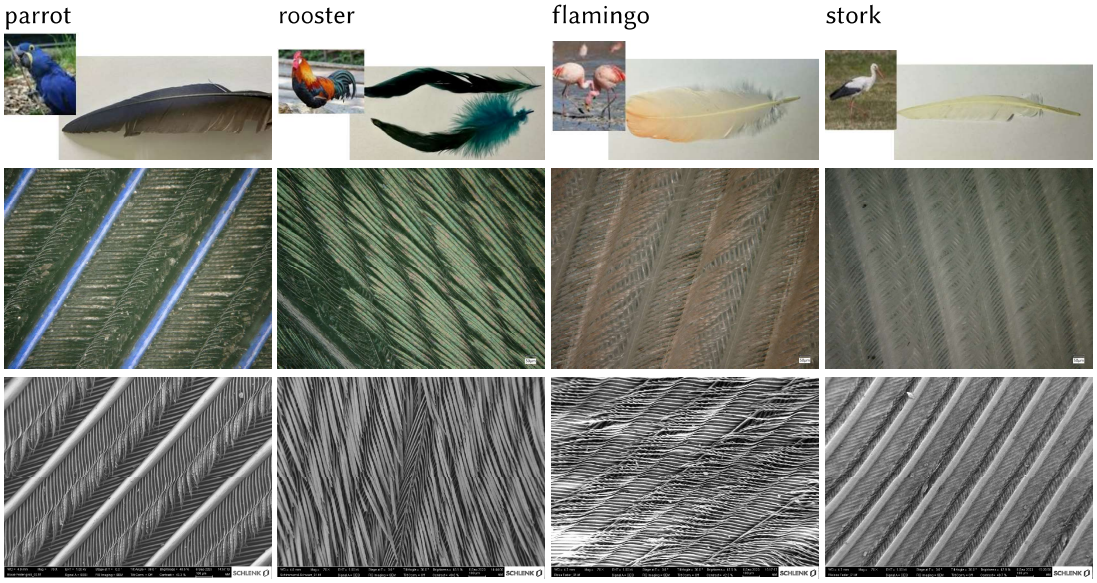

Figure 4: Four feather samples were analyzed in our study. Detailed structural images of these samples were obtained using light microscopy (second row) and scanning electron microscopy SME (third row).

All feathers have distinctly different colors and structures, as shown in the light and scanning electron microscopy (SME) images in the second and third rows of Fig. 4. These images clearly display the varying topology and shape of barbules. While the flamingo and stork have their coloration based on absorption pigments [1], the parrot and rooster also include structural coloration.

In natural feathers, blue coloration, such as that in macaw parrot feathers Fig. 3, is structural, resulting from a unique porous structure in the barbs with dimensions smaller than the wavelength of light. The smaller barbules branching from these barbs retain their dark coloration because they lack this particular structure. Some species combine both absorption and structural colors, such as creating green by combining yellow absorption pigment with structural blue.

The Cochin cock features a green absorption pigment, a mixture of black and yellow compounds, giving it an olive green color. Green or possibly violet reflections result from structural variations in the keratinized surface of the feathers and are not due to a pigment different from the usual present pigments. The high glossiness of these feathers is due to melanin, which has a very high index of refraction [15], greater than that of the surrounding keratin. Single structures of eumelanin are iridescent, endowed with metallic-like colors that change according to the angle of illumination.

4. Appearance Capture

To gain insight into the angle-dependent behavior of our feather specimens, we captured the specimen surfaces using the SIGHTTEX Q goniometric device. This device is based on a goniometric setup utilizing two arms outfitted with five RGB cameras and 28 non-polarized LED lights, both positioned approximately 300 mm from the measured area, which has a maximum size of 40 $\times$ 40 mm. The device allows for capturing arbitrary azimuthal angles, while polar angles are fixed at 15-degree intervals up to 75 degrees. The captured high dynamic range images of a 3$\times$3 mm feather patch, with a resolution of 1500 DPI, have a size of 237 $\times$ 237 pixels.

We captured several types of data. First, we used in-plane analysis, a standard method for characterizing the scattering of isotropic materials. During this measurement, the view was fixed at 45 degrees, and the light varied between -81 and 81 degrees at 3-degree intervals, resulting in 55 captured images. Next, we captured the full view- and illumination-dependent texture of the samples using the bidirectional texture function (BTF) [16]. Both illumination and viewing directions were sampled in 15-degree steps in polar angle and 30-degree steps in azimuths, resulting in 3660 captured images. The capturing time was approximately 30 minutes. We also captured different patches of feathers, resulting in very similar appearance data when the alignment of the barbules was constant.

5. Angle-Dependent Analysis

5.1. Inplane Analysis

As feathers are highly anisotropic due to their structure, the in-plane analysis of feather samples is highly dependent on the orientation of the captured plane relative to the sample. We used a similar orientation of the plane to the barbs (the plane perpendicular horizontally to the captured barb structure), as shown in Fig. 5.

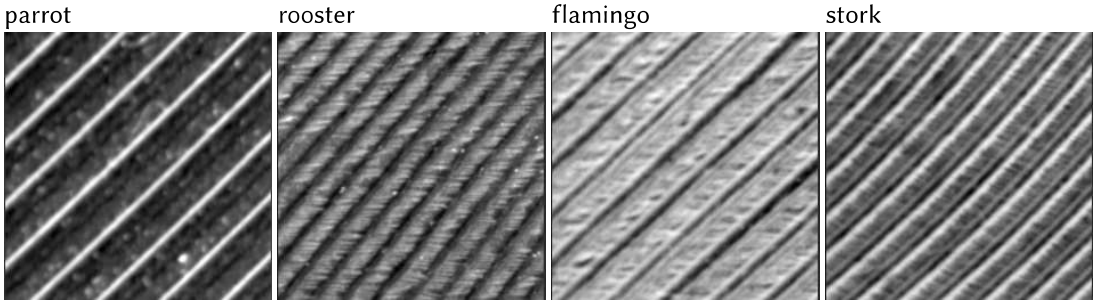

Figure 5: Samples luminance for a diffuse illumination obtained from the measurements (captured area 3$\times$3 mm).

The results of our analysis in CIE L*a*b* are shown in Fig. 6. Fig. 6-a presents luminance as a function of illumination angle, highlighting the retro-reflection and specular reflection directions. We do not observe any sharp peaks at the specular reflection direction due to the overall diffuse nature of the samples. Only the parrot and flamingo samples exhibit a stronger

increase in luminance in this direction. In the flamingo feather, we observe a relatively wide peak, while the parrot shows a narrower peak slightly offset from the ideal specular direction. This is likely due to the fact that the specularity arises from the protruding cylindrical structure of barbs with a porous structure that induces blue structural color in the retro-reflective region but exhibits bright highlights at specular directions. In the retro-reflective direction, peaks can only be observed for samples that include some structural colors, i.e., parrot and rooster. In the case of the parrot, such peak is actually of higher intensity than the specular one.

We also compared color changes due to the change of in-plane illumination direction. Fig. 6-b shows an a*-b* chart including all the samples, and it is evident that the only sample exhibiting significant color changes is the parrot, moving from dark achromatic hues to strong structural blue.

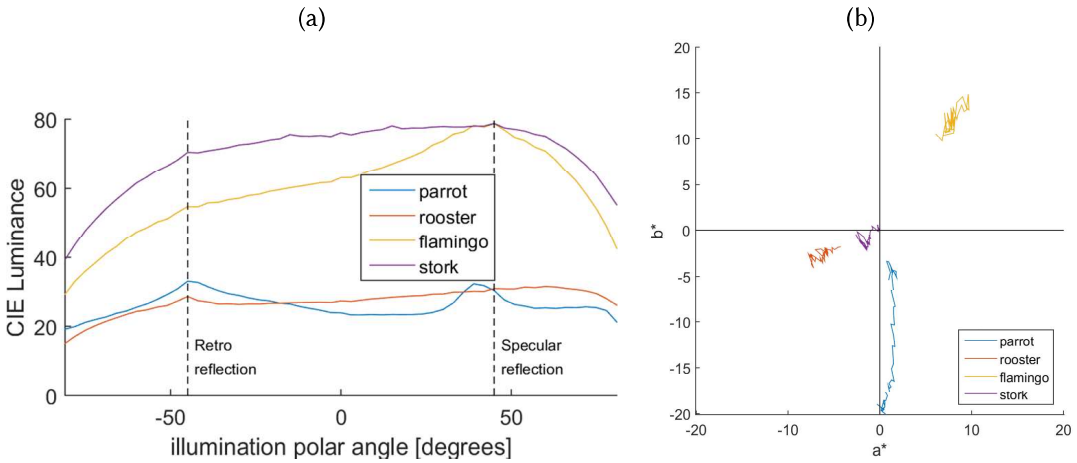

Figure 6: In plane CIE (a) luminance and (b) color a*b* chart of the tested feathers.

5.2. Uniform angle-dependent measurements

Angle-dependent appearance measurements sampled uniformly over the hemisphere of incoming and outgoing directions provide ample information useful for appearance analysis and visualization in virtual environments. Fig. 7 provides an overview of the geometries captured. It represents each of the 3660 captured images by their average color as a single pixel, forming an image where rows correspond to 61 illumination directions and columns to 60 viewing directions. This image displays values of the bidirectional reflectance distribution function (BRDF) [17] and demonstrates the material's reflectance distribution as a function of illumination (rows) and viewing (columns) directions, moving circularly from the pole of the hemisphere above the material to its bottom. Polar angles are sampled in 15° steps (for light 0°, 15°, 30°, 45°, 60°, 75°; for view 15°, 30°, 45°, 60°, 75°). Within each polar angle, 12 azimuthal angles are sampled. This BRDF image provides a fingerprint of the material's angle-dependent behavior and reveals specific characteristics such as color intensity, presence and strength of anisotropy, and strength of specular reflection. A comparison of the BRDFs of our feather samples is shown in the first row of Fig. 8. When we compare these BRDF images with similar images obtained for a single

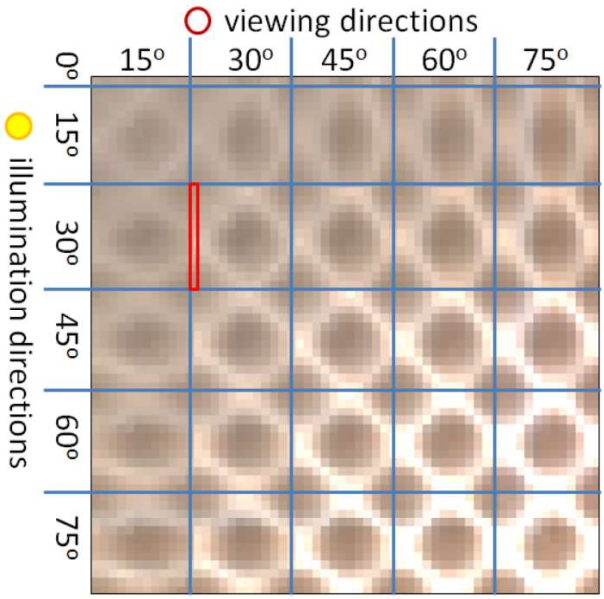

Figure 7: An overview of captured angle-dependent data, where each pixel represent average color of one captured image, visualizing four-dimensional BRDF function in a two-dimensional image.

image pixel in the second row, we can see clear differences due to local view occlusion and masking effects, exhibited by vertical stripes. This occurs when a part of the feather, such as a barb, is higher than its surroundings, as is clearly visible in the image of the parrot sample, which has barbs slightly protruding from the feather plane. Due to these effects, the data do not fulfill BRDF assumptions and are often referred to as apparent BRDFs (ABRDF). The last two rows show the minimal and maximal values in the captured images. Again, the strongest difference is observed in the parrot, showing a contrast between pixels representing structural blue barbs and darker areas between barbules. This difference is also visible for the rooster but is less prominent for the flamingo and stork.

When examining detailed surface behavior at specific geometries, we can analyze individual images. For our analysis, we selected low polar angles 30° to avoid large perspective foreshortening of the feather samples' structure and analyzed the samples' behavior for a fixed viewpoint and varying illumination azimuths at the same polar angle. These twelve geometries are illustrated by the red rectangle in the BRDF image in Fig.7. Fig.9 shows the corresponding twelve captured images arranged azimuthally around an image showing feather structure obtained by SME. The azimuthal arrangement corresponds to the azimuthal direction of illumination and provides an intuitive explanation of light interaction with the feather structure.

Let's observe the texture of the samples in more detail. The parrot sample, at retro-reflective directions (where the light and camera are close enough), exhibits strong structural blue at the barbs, while the barbules become very dark. At near-specular directions, we observe specular highlights from the barbs, indicating they likely have a smooth, glossy surface. Additionally, the barbules become brighter, with a clear boundary between two touching rows of structures. This behavior is supported by the sample's BRDF in Fig. 8, showing structural blue and gray

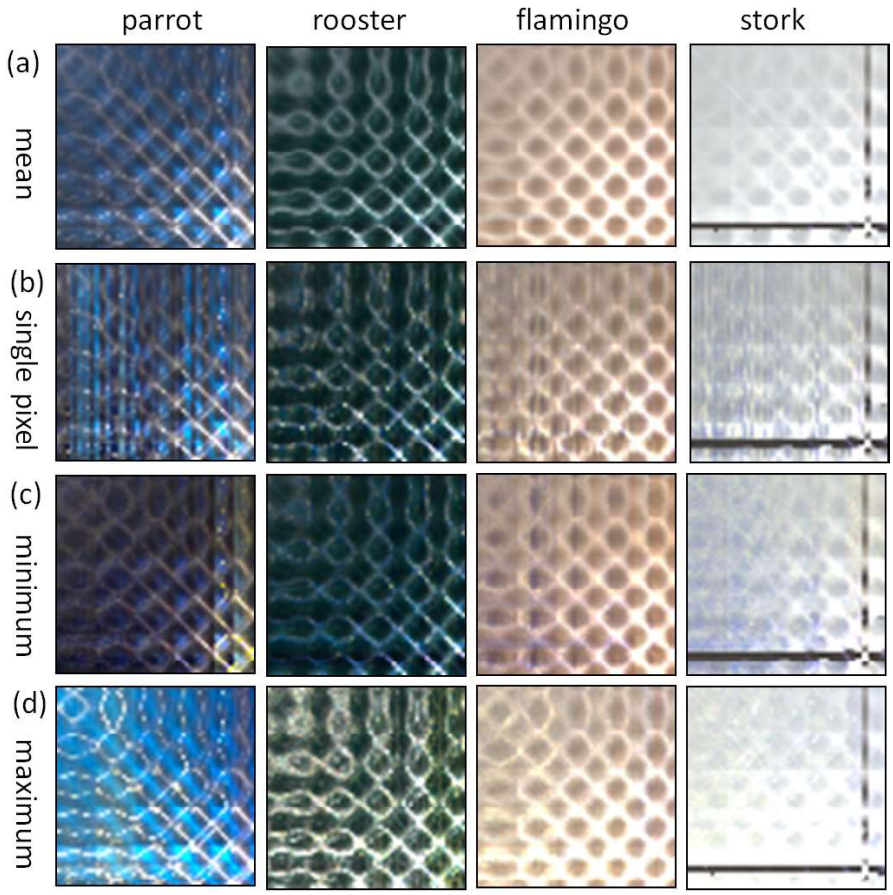

Figure 8: A comparison of BRDFs obtained as by images averaging (the first row), as a value of a single pixel (the second row), as minimal and maximal image values (the third and fourth row).

anisotropic reflection as the main visual features.

The rooster's sample BRDF shows strong anisotropic behavior as the main visual feature, driven by the orientation of the barbules. The rooster's barbules have a larger area, making them more effective reflectors of incoming light. Consequently, this sample is not the brightest at specular directions but at directions where the barbules are properly oriented relative to the light and camera.

Similarly to the rooster, the flamingo sample does not show barbs but has two layers of barbules, one slightly above the other. The main visual feature is the increased contrast between these two layers at specular directions, where only the upper layer participates in light transmission. A very similar effect is observed in the stork sample, which has a similar structure topology to the parrot; however, as it lacks structural color, the main visual effect is the increased contrast between differently oriented regions of barbules. The BRDFs in Fig. 8 for all the last three samples show anisotropic reflection from oriented barbules as the major visual behavior.

As the captured illumination and viewing angle-dependent data represent a bidirectional texture function (BTF), they can be readily used for sample visualization. Fig. 10 shows a visualization of the captured physical area (3×3 mm) on a blob-like object. The first row shows

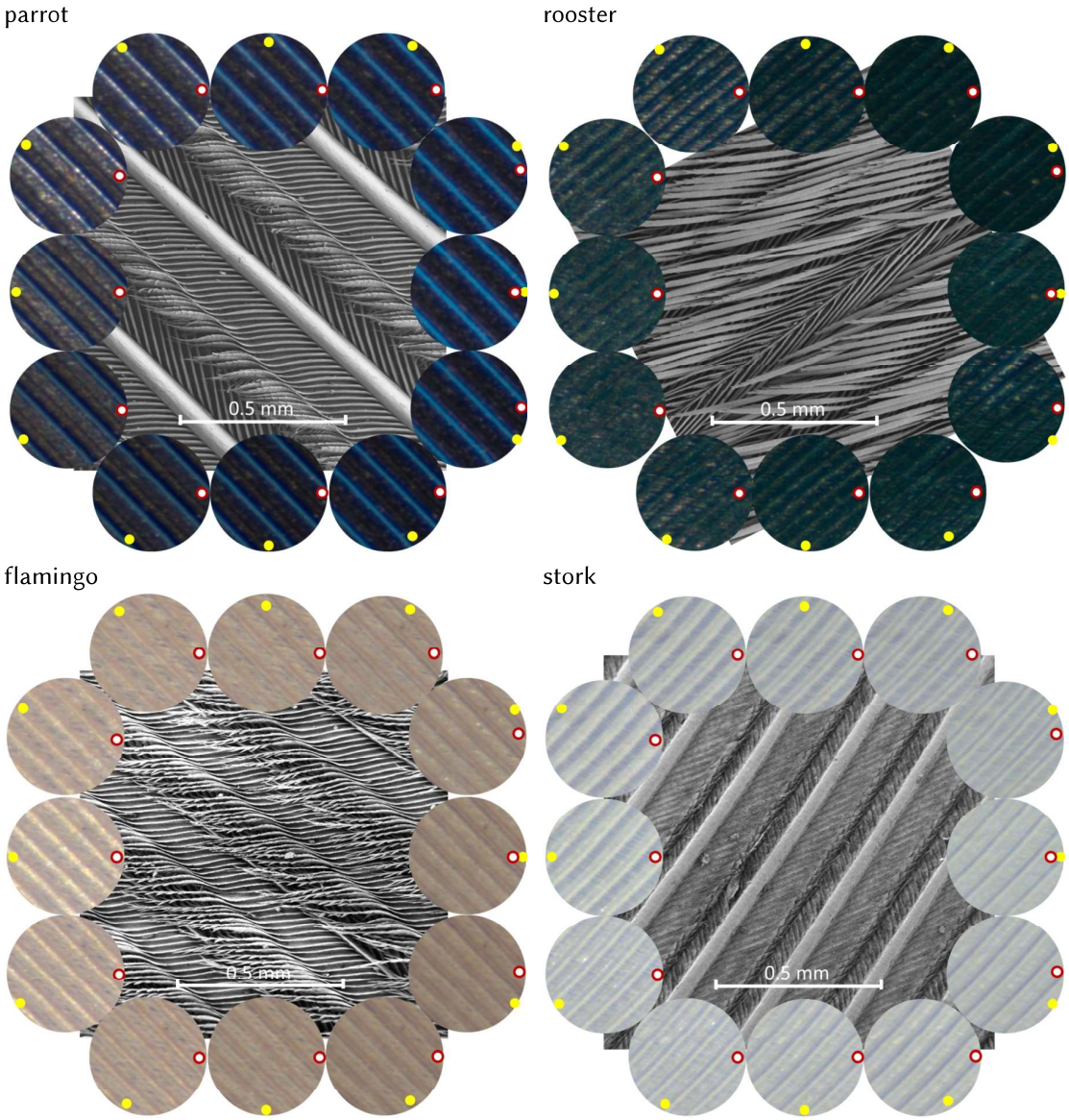

Figure 9: Feather local structure change as a function of illumination azimuthal direction for view and illumination polar angles fixed to 30°. Yellow and white dots denote illumination and viewing azimuths. The inset image shows a structure details obtained using SME.

frontal (retro-reflective) illumination, while the second row shows the object illuminated from the left. These two lighting conditions clearly demonstrate the retro-reflective properties of the parrot sample's structural blue, as well as the anisotropic highlights of the rooster and flamingo samples.

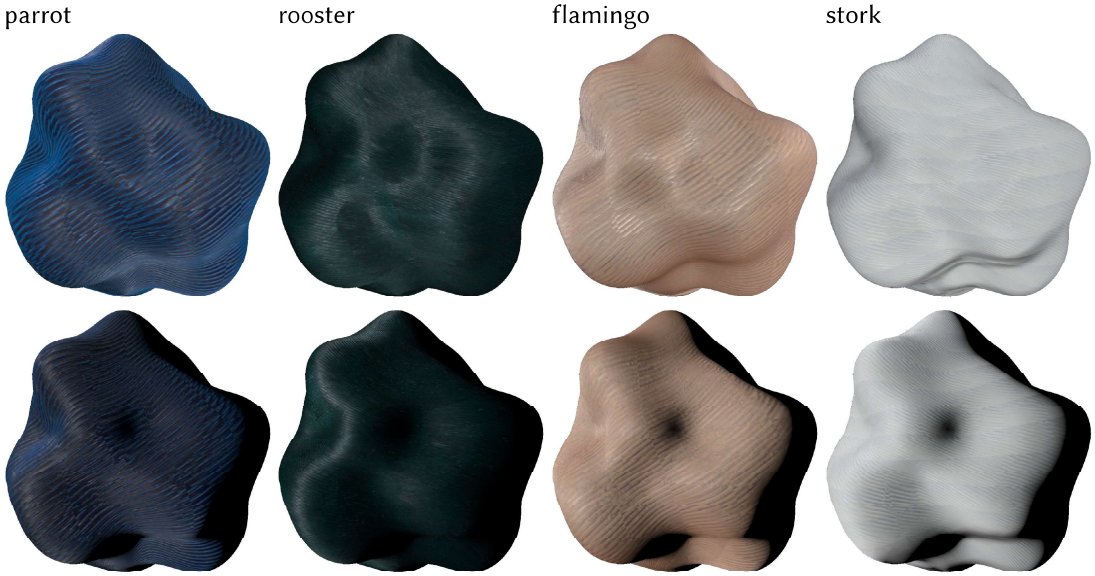

Figure 10: Feather samples were visualized using BTF on a 3D object under both frontal and side illumination. This visualization effectively demonstrates the angle-dependent properties, showcasing retro-reflective properties and anisotropic highlights.

6. Angular behavior modelling

As shown in Fig. 8, the main visual features of captured BRDFs include anisotropic, retro-reflective, and specular highlights. While the locations of the latter two are clearly defined by the mutual azimuthal positions of light and camera, the locations of anisotropic highlights are quite non-intuitive, forming an intricate pattern in the BRDF angular space.

However, the locations of anisotropic in angular domain can be reliably predicted on directional surface elements, laying in planes orthogonal to the bisector (often denoted as the half-way direction $\mathbf{H} = \frac{\omega_i+\omega_v}{||\omega_i+\omega_v||}$) of directions of the incidence $\omega_i = [\theta_i, \varphi_i]$ and reflectance $\omega_v = [\theta_v, \varphi_v]$ directions, as proposed in [18]. Therefore, the anisotropic highlights can be predicted [19] at directions of the bisector that are orthogonal to the anisotropic angle φ_a of the material $\mathbf{U} = [\sin\varphi_a, \cos\varphi_a, 0]$. Thus, the angular locations of anisotropic highlights can be expressed as

$$\begin{aligned} F(\varphi_a) &= 1 - |\mathbf{H} \cdot \mathbf{U}(\varphi_a)| \\ \mathbf{U}(\varphi_a) &= [\sin\varphi_a, \cos\varphi_a, 0] \end{aligned} \tag{1}$$

To account for areas of anisotropic highlights, we generate a support mask M around the highlights as shown in Fig. 11-2. The support mask M with a smooth boundary can be expressed as a function of anisotropic angle φ_a, width of anisotropic highlight w, and width of its smooth edge d_w as follows

$$M(\varphi_a, w) = \begin{cases} 1 & x \leq w - d_w \\ 0 & x \geq w + d_w \\ f(x) & w - d_w < x < w + d_w \end{cases}$$

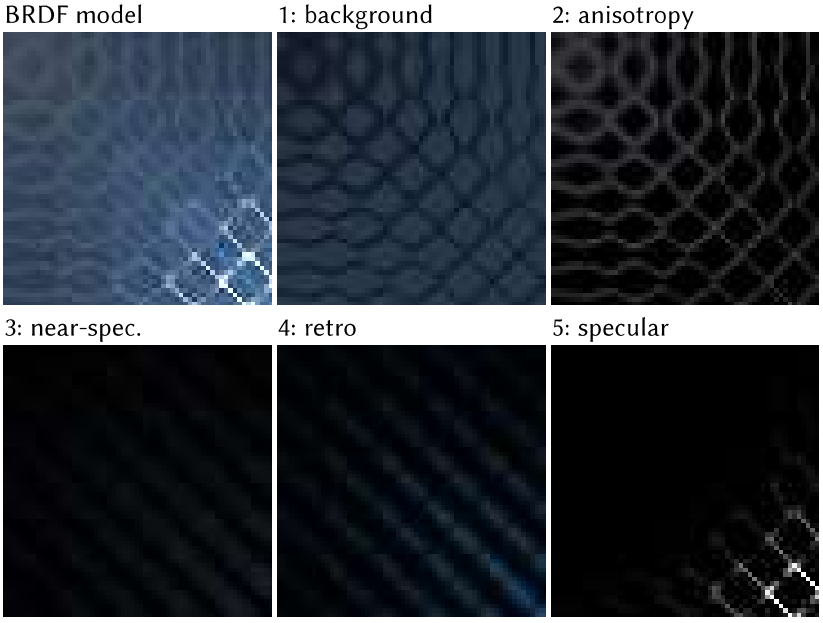

Figure 11: Illustrative decomposition of the proposed BRDF model (parrot) into its five additive factors: (1) constant background, (2) anisotropic highlight, (3) near-specular highlight, (4) retro-reflective highlight, and (5) specular highlight.

where $x = 1 - |\mathbf{H} \cdot \mathbf{U}(\varphi_\mathbf{a})|$, and $f(x)$ is a smoothstep function $f(x) = y^2(3 - 2y)$ where $y = \frac{x-w+d_w}{2d_w}$.

Our BRDF model is composed of five additive factors each accounting for (1) constant background, (2) anisotropic highlight, (3) near-specular highlight, (4) retro-reflective highlight, and (5) specular highlight, as shown in Fig. 11. Therefore, the model can be expressed using five additive terms constrained by support areas defined by mask M or out of it using its complement $(1 - M)$

$$\begin{aligned} f(\omega_i, \omega_v, j) &= (1 - M) \cdot \mathbf{C}_b(j) + \\ &+ M \cdot \mathbf{C}_a(j) + \\ &+ (1 - M) \cdot \mathbf{C}_s(j) \cdot E \cdot D(0) \cdot F + \\ &+ (1 - M) \cdot \mathbf{C}_r(j) \cdot E \cdot D(\pi)^\gamma \cdot F + \\ &+ M \cdot \alpha E^\beta \cdot D(0) \ , \end{aligned} \tag{2}$$

(3)

where j is the RGB channel index, C_b, C_a, C_s, and C_r denote background, anisotropic highlight, near specular, and retro-reflective RGB color. The parameters α and β perform elevation-dependent scaling of the cosine factor defined as

$$E = 1.1 - \cos\theta_i \cos\theta_v \ . \tag{4}$$

A normalized difference of azimuthal angles represents the shape of the azimuthally dependent

lobe specified by angle δ (0 for specular lobe, π for retro-reflective lobe):

$$D(\delta) = \frac{|\varphi_i - \varphi_v - \delta|}{2\pi} \quad . \tag{5}$$

Finally, the width of the retro-reflective lobe is specified by parameter γ, and factor F accounts for the decrease of retro-reflective intensity for different elevations of light and camera as follows:

$$F = 1 - \frac{|\theta_i - \theta_v|}{\theta_{max}} \quad , \tag{6}$$

where θ_{max} specifies the maximum elevation angle captured in the data, in our case 75°.

We fitted our model to the captured BRDFs of individual feather samples and obtained the parameters outlined in Tab. 1. A comparison of the captured and fitted BRDFs is given in the first two rows of Fig. 12. Rendering of the respective variants on a bird shape model illuminated from the frontal direction is shown in the third and fourth row of the same figure, while the fifth row shows the difference. From the rendering it is clear that model well preserves the main visual the tested features and represents satisfactory simulation of their angle-dependent appearance.

The meaning of the model's parameters is quite intuitive. They define the direction of anisotropy φ_a, and the colors of the background C_b, anisotropic highlights C_a, near-specular highlights C_s, and retro-reflective highlights C_r. The remaining parameters $\alpha, \beta, \gamma, w, d_w$ shape the width and intensity of individual highlights. For the purpose of this paper, the parameters were tuned manually. However, due to the model's close-form definition, they can be easily fitted using a non-linear fitting method, such as the steepest descend. The analytical definition of the model also allows for its fast evaluation, enabling the OpenGL rendering in Fig. 12 to run at speed of 20 FPS on a PC with an Intel Core i7.

7. Conclusions

This paper analyzed the angle-dependent optical properties of four feather samples, one of which included structural color. By analyzing in-plane behavior, BRDF, and BTF data, we highlighted the differences between optical properties of the samples and suggested the reasons for this behavior. Finally, we proposed an analytical BRDF model that reproduces feather sample's reflectance behavior based on a few intuitive parameters. A shader function of the model is publicly available at the project website https://staff.utia.cas.cz/filip/pub.html.

8. Acknowledgements

This research has been supported by the Czech Science Foundation grant GA22-17529S. We thank Heidi & Hans-Jürgen Koch for providing pictures depicting the angle-dependent appearance of feathers in Fig.2.

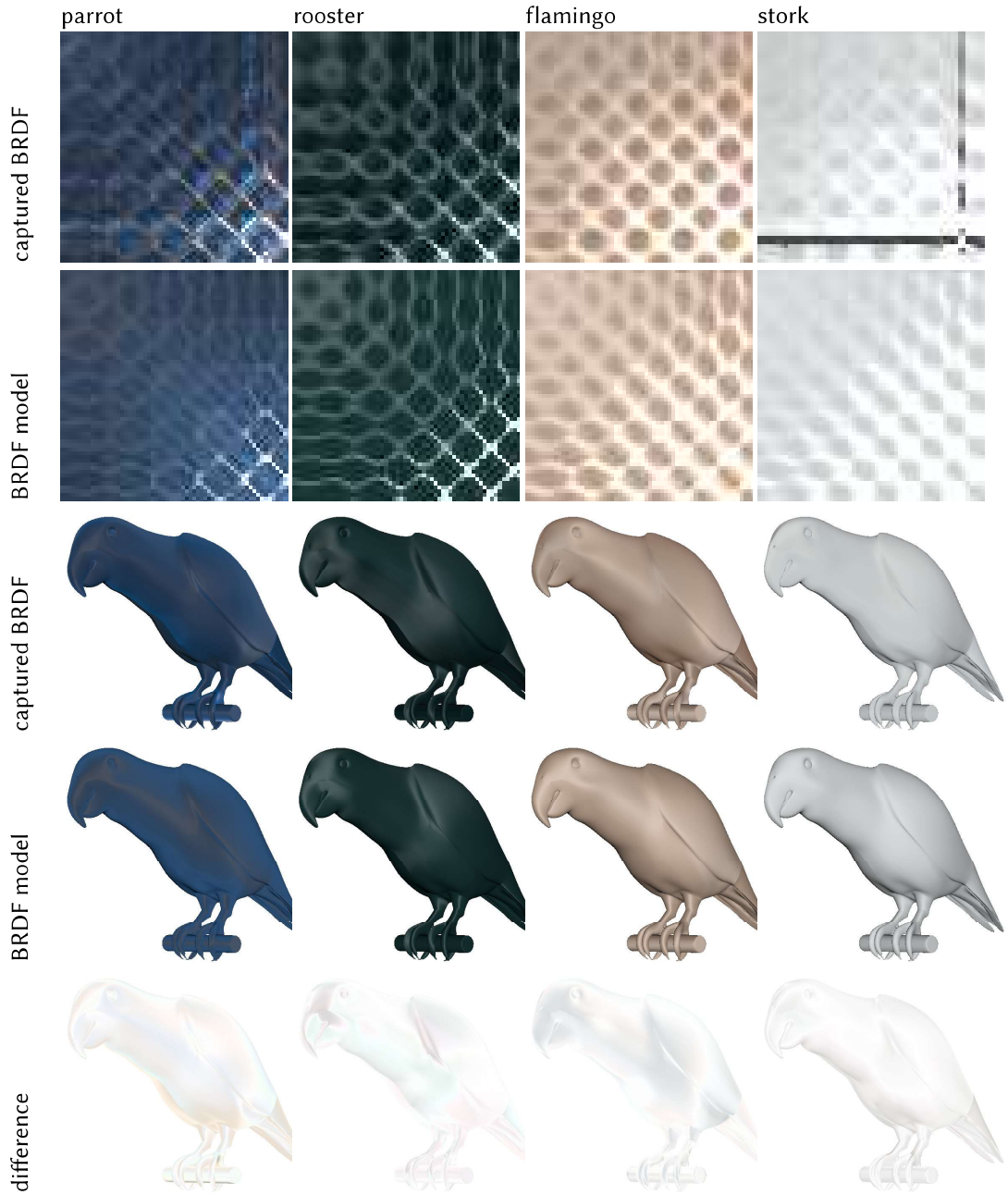

Figure 12: A comparison of the captured BRDF and its fit using the proposed BRDF model. The quality of the fit is illustrated by rendering a bird shape illuminated from a frontal direction, visualizing angle-dependent effects of feather samples on a complex geometry.

References

[1] F. J. Maile, G. Pfaff, P. Reynders, Effect pigments-past, present and future, Progress in organic coatings 54 (2005) 150–163.

[2] . Britannica The Editors of Encyclopaedia, feather, https://www.britannica.com/science/feather. accessed 13 may 2024, 2024.

[3] H. Koch, H. J. Koch, Federn, poetisches meisterstück der evolution, Frederking & Thaler Verlag, 2023. doi:https://heidihanskoch.com/.

[4] I. Newton, Opticks, or, a treatise of the reflections, refractions, inflections & colours of light, Courier Corporation, 1952.

[5] W. D. Bancroft, Structural colours in feathers., Nature 112 (1923) 243–243.

[6] G. Pfaff, P. Reynders, Angle-dependent optical effects deriving from submicron structures of films and pigments 99 (1999) 1963–1981.

[7] M. Srinivasarao, Nano-optics in the biological world: beetles, butterflies, birds, and moths, Chemical reviews 99 (1999) 1935–1962.

[8] H. Gruson, M. Elias, C. Andraud, C. Djediat, S. Berthier, C. Doutrelant, D. Gomez, Hummingbird iridescence: an unsuspected structural diversity influences colouration at multiple scales, BioRxiv (2019) 699744.

[9] R. Maia, L. D'Alba, M. D. Shawkey, What makes a feather shine? a nanostructural basis for glossy black colours in feathers, Proceedings of the Royal Society B: Biological Sciences 278 (2011) 1973–1980.

[10] V. Saranathan, J. D. Forster, H. Noh, S.-F. Liew, S. G. Mochrie, H. Cao, E. R. Dufresne, R. O. Prum, Structure and optical function of amorphous photonic nanostructures from avian

Table 1
Parameters of the fitted BRDFs.

par.		parrot	rooster	flamingo	stork
$\varphi_a[^\circ]$		90.0	-20.0	-80.0	-20.0
$\mathbf{C}_b$	R	0.155	0.089	0.701	0.792
	G	0.214	0.198	0.607	0.809
	B	0.290	0.194	0.535	0.812
$\mathbf{C}_a$	R	0.390	0.344	0.891	0.874
	G	0.384	0.413	0.819	0.888
	B	0.416	0.415	0.768	0.888
$\mathbf{C}_s$	R	0.206	0.104	0.961	0.422
	G	0.285	0.190	0.851	0.429
	B	0.387	0.187	0.771	0.429
$\mathbf{C}_r$	R	0.107	0.089	0.779	0.792
	G	0.277	0.198	0.674	0.809
	B	0.446	0.194	0.595	0.812
α		3.0	5.0	5.0	5.0
β		12.0	12.0	5.0	5.0
γ		4.0	0.0	0.0	0.0
w		0.95	0.85	0.80	0.80
d_w		0.40	0.20	0.40	0.60

feather barbs: a comparative small angle x-ray scattering (saxs) analysis of 230 bird species, Journal of The Royal Society Interface 9 (2012) 2563–2580.

[11] A. J. Parnell, A. L. Washington, O. O. Mykhaylyk, C. J. Hill, A. Bianco, S. L. Burg, A. J. Dennison, M. Snape, A. J. Cadby, A. Smith, et al., Spatially modulated structural colour in bird feathers, Scientific reports 5 (2015) 18317.

[12] M. Imafuku, N. Ogihara, Wing scale orientation alters reflection directions in the green hairstreak chrysozephyrus smaragdinus (lycaenidae; lepidoptera), Zoological science 33 (2016) 616–622.

[13] A. Saito, Material design and structural color inspired by biomimetic approach, Science and technology of advanced materials 12 (2012) 064709.

[14] S. Magkiriadou, J.-G. Park, Y.-S. Kim, V. N. Manoharan, Disordered packings of core-shell particles with angle-independent structural colors, Optical Materials Express 2 (2012) 1343–1352.

[15] W. Li, A. Patil, X. Zhou, Z. Wang, M. Xiao, M. D. Shawkey, N. C. Gianneschi, A. Dhinojwala, Characterization of broadband complex refractive index of synthetic melanin coatings and their changes after ultraviolet irradiation, Applied Physics Letters 117 (2020).

[16] K. Dana, B. van Ginneken, S. Nayar, J. Koenderink, Reflectance and texture of real-world surfaces, ACM Trans. on Graphics 18 (1999) 1–34.

[17] F. Nicodemus, J. Richmond, J. Hsia, I. Ginsburg, T. Limperis, Geometrical considerations and nomenclature for reflectance, NBS Monograph 160 (1977) 1–52.

[18] R. Lu, J. J. Koenderink, A. M. Kappers, Specularities on surfaces with tangential hairs or grooves, Computer Vision and Image Understanding 78 (2000) 320–335.

[19] B. Raymond, G. Guennebaud, P. Barla, R. Pacanowski, X. Granier, Optimizing BRDF orientations for the manipulation of anisotropic highlights, in: Computer Graphics Forum, volume 33, Wiley Online Library, 2014, pp. 313–321.